A Novel Electrochemical Sensor Based on a Graphene-Silver Platform for the Sensitive Determination of a Tumor-Supplied Group of Factors

Yan Zhang[1] and Guohong Li[2]*

[1] Department of Neurology, Yinan County People's Hospital, Shandong, 276300, P.R. China
[2] Department of Laboratory, Dezhou Municipal Hospital, No. 1766 Middle Sanba Rd, Decheng, Dezhou, Shandong, 253012, P.R. China
[*]Corresponding author: Yan Zhang E-mail: Lghhappy111@sina.com

This work reported the facile fabrication of a silver nanoparticle (AgNP)/graphene oxide (GO)-based nanocomposite with glucose as a reducing and stabilization agent using an eco-friendly and low-cost method. The synthetic process could be conveniently employed in the fabrication of a disposable electrochemical sensor using a glassy carbon electrode (GCE). Based on the experimental results, this nanocomposite displayed the integrated properties of graphene and silver nanoparticles, which significantly promoted its electrocatalytic behavior. The electrochemical features of the AgNPs/GO/GCE with the tumor-supplied group of factors (TSGF) was evaluated by differential pulse voltammetry (DPV) and cyclic voltammetry (CV). Compared with the GO film, the AgNPs/GO film displayed an obviously higher activity for TSGF electro-oxidation with a tenfold enhancement in the peak current. Under the selected test conditions, the oxidation peak currents were found to be proportional to the concentration of TSGF within the ranges of 0.01 μM - 50.0 μM and 50.0 μM - 800.0 μM. The developed sensor was used for the detection of TSGF in real specimens and showed desirable recoveries in the range of 98.18% - 102.52%.

Keywords: Silver; Graphene; Tumor supplied group of factors; Electrochemical sensor; Human serum

1. INTRODUCTION

Brain cancer is the most common form of human cancer and was listed as the fourth highest fatal cause associated with malignant diseases in humans, following lung cancer [1, 2]. Recently, there has been a sharp increase in the occurrence of brain cancer in Eastern and Western countries. Therefore, a large number of investigations around the globe have been carried out to determine the most effective methods of brain cancer treatment, therapeutic effect evaluation, correct prognosis evaluation and postoperative recurrence identification in patients [3-5]. Currently, mammography is a

common technique used for early determination and has been proven to be poorly sensitive to the determination of tumors in dense brain tissue. Nevertheless, the easily performed blood test can avoid the imaging-involved issue of high brain density [6]. In addition, blood testing could benefit the younger women that are currently not included in most brain cancer screening programs, primarily since dense brain tissue is rather prevalent in this group [7]. Components in bodily fluids can be easily detected and are regarded as perfect biomarkers for the diagnoses of diseases. For instance, cancer antigen 15-3 (CA15-3), carcinoembryonic antigen (CEA), cancer antigen 125 (CA125) and other cancer biomarkers have been reported [8, 9]. Nevertheless, protein biomarkers similar to these are ordinarily not adequately sensitive for use in screening and early diagnosis since their levels are indicative of the tumor burden [10]. Blood-brain barrier autoantibodies discharged against tumor antigens have been regarded as potential biomarkers for early cancer diagnosis since they can be detected even in the case of extremely small tumors, which is different from the case of conventional tumor biomarkers [11]. In addition, compared with protein markers, which have to be detected with two varied monoclonal antibodies, nipple discharge components can be easily detected via target antigens and secondary reagents. Thus, a multiplex tumor-associated autoantibody measurement can be easily constructed using the latter. Nevertheless, the few available biomarkers employed in the early determination of brain cancer have been found to have poor diagnostic specificity and sensitivity in stand-alone detection attempts [12-14]. Hence, compared with a single biomarker, a panel of biomarkers might be a better prediction method. Furthermore, a panel of several biomarkers might be required for the determination of the various subtypes of brain cancer since it is a heterogeneous disease [15]. Extensive investigation into the combinations of biomarkers to explore their effectiveness in early brain cancer determination has not been performed [16, 17], though several investigations have studied the behavior of a panel of cancer biomarkers in comparison with a single biomarker alone [18-21].

Tumor supplied group of factor/tumor specific growth factor (TSGF) was the first *in vitro* tumor marker. In addition, its kit was initially approved by the Chinese government. As a marker secreted by cancer cells, TSGF is gradually released into the blood during cancer formation and growth and could facilitate the growth and angiogenesis of malignancies [22]. According to diverse reports from various organizations in China, TSGF has been found to be highly sensitive for the determination of malignant tumors, such as colorectal carcinoma, nasopharyngeal carcinoma, and pancreatic cancer, particularly for detection of the malignancy at an early stage. Jiang and co-workers assessed the diagnostic value of TSGF in the serum of 96 patients suffering from brain cancer and proposed that the positive and negative likelihood ratios, specificity and sensitivity were 5.4, 0.10, 83.0% and 91.6%, respectively [23]. In addition, compared with CA19-9 and CA242, TSGF in stage I of the disease displayed a remarkably higher sensitivity for brain cancer diagnosis ($P < .01$).

A colorimetric biochemistry kit is a common technique used for the determination of the TSGF level. Nevertheless, colorimetric measurement has its own disadvantages, including poor accuracy and sensitivity. To offset these inherent demerits, an electrochemical technique is a desirable substitute because of its favorable sensitivity and sophisticated analysis. In particular, the electrochemical method provides a wide dynamic range. In addition, this method only requires small specimen volumes (usually in the microliter range), corresponding to a low LOD; thus, the analyte can be

detected at sub-picogram levels. Nevertheless, it has been confirmed that the direct electrochemical oxidation of TSGF is kinetically sluggish. In addition, this method requires a comparatively high overpotential for the oxidization of TSGF at a bare electrode. Hence, the working electrodes used in conventional electrochemical systems are usually surface-modified to achieve a decrease in the overpotential and an enhanced electrochemical response to the target molecules [24-28].

As a new member of the carbon materials group, graphene is a two-dimensional sheet of carbon atoms bonded through sp^2 hybridization. Since graphene possesses a large specific surface area, desirable mechanical and thermal features, excellent electrical conductivity and other new features, it can provide versatile selective catalytic or sensing behaviors; thus, it has been regarded as a perfect two-dimensional catalyst support for anchoring semiconductor and metal catalyst nanoparticles [29]. Nevertheless, if graphene sheets are not well separated from each other, agglomerates are irreversibly formed, or the sheets can even restack to form graphite under Van der Waals interactions. Any variation in the solution, including the addition of acids, salts or organic dispersants, causes aggregation, which limits the preparation of diverse graphene composites and the utility of graphene sheets. Oxidized graphene, also termed graphene oxide (GO), has a two-dimensional plane and many oxygen-containing functional groups, with disorder on the basal planes and edges [30]. This material is desirably dispersible and film-forming and inherits the features of graphene. The excellent molecular-level chemical sensing capability and mechanical strength are ascribed to the covalent oxygen functional groups in GO[31, 32]. GO is not only characterized by the nature of the atoms on its surface, but it can also be prepared in a scalable solution-based process, and it is well-known to have a controllable surface defect density for modulation of the sensor specificity and sensitivity; hence, GO is remarkably suited to application in biological and chemical sensors [33]. Nanocomposites based on nanosized inorganic particles and clusters have the potential to modify and optimize the features of the terminal materials for diverse uses, so they have been a study focus. Silver nanoparticles (AgNPs) have been applied in bactericidal agents and biosensor fabrication owing to their high quantum characteristics of a large specific surface area and small granule diameter, along with the capacity for strong antibacterial activity and fast transfer of that activity [34].

This work proposed a simple synthesis of AgNPs/GO through the reduction of silver ions on the surface of GO with glucose as the reduction and stabilization agent. Thereafter, the AgNPs/GO was employed for the fabrication of a new electrochemical sensor for TSGF detection. This sensor was characterized by a sensitive current response since it not only provided a large electrochemically active surface area for TSGF adsorption but also significantly promoted electron exchange between the solution and electrode. The successful and selective detection of TSGF in a serum specimen was achieved by the proposed sensor.

2. EXPERIMENTS

2.1. Chemicals

Graphite powder (320 mesh, spectrum pure), H_2O_2 (30 wt%), $KMnO_4$ and H_2SO_4 commercially available in Shanghai Chemical Reagent Co. were employed for GO synthesis. Uric acid and TSGF

were commercially available in Sigma–Aldrich. $AgNO_3$, $NH_3 \cdot H_2O$, ascorbic acid and glucose were obtained from Alfa Aesar. The right amount of TSGF was dissolved in the dilute HCl for the daily preparation of TSGF standard stock solutions (1.0 mM). The supporting electrolyte was an acetate buffer (0.1 M, pH 4.5). All other chemicals were of analytical reagents grade and used without further purification. Double-distilled water was used in all tests.

2.2. Synthesis of AgNPs/GO nanocomposite

A modified Hummers method was employed for the synthesis of GO from natural graphite powder [35]. The synthesis of the AgNPs/GO nanocomposite was achieved by the direct reduction of silver ions on GO using glucose as a reducing reduction and stabilization agent. The following procedure illustrates the characteristic preparation route of the nanocomposite: After the dispersion of 5.0 mg of GO powder in 5.0 mL of water under sonication for 60 min, a stable GO colloid was obtained. This was followed by the dissolution of 0.25 g of glucose in the dispersion and stirring. Then, 0.5 M ammonia was added into 1.0 mL of a silver nitrate aqueous solution (5 mM) until the $AgOH/Ag_2O$ precipitate dissolved. Then, the GO- and glucose-containing solution was introduced into the obtained $Ag(NH_3)_2OH$ solution, which was stirred for 30 min. In addition, the mixed solution was left to stabilize for 2 h at ambient temperature. The terminal product was slurry-like. After centrifugation, this product was repeatedly washed with water for the removal of any possible impurities. The yielded product was left to dry in an oven at 60 °C to obtain the AgNPs/GO nanocomposite.

2.3. Sensor fabrication

After mechanical polishing with 0.3and 0.05 mm alumina slurry and successive sonication in dilute nitric acid, anhydrous ethanol and redistilled water for 15 min, the GCEs were left drying under nitrogen stream. DMF solution (2.5 mL) was mixed with AgNPs/GO (5.0 mg), and subjected to ultra-sonication for 0.5 h to obtain a stable suspension. 5.0 μL of this mixture was casted to the surface of GCE using a micropipette, and left drying completely under an infrared lamp. This was followed by repeatedly rinsing the modified electrode using distilled water, which was later left air-drying for further use. The terminal electrode was AgNPs/GO/GCE. By contrast, the same procedure proposed above was used for the preparation of GO/GCE nanocomposite with only GO.

2.4. Characterizations

A Renishaw inVia plus Raman microscope with a 514.5 nm argon ion laser and an FTIR-8700 spectrometer (Shimadzu, Japan) using the KBr pressing plate method were used to obtain Raman spectra and Fourier transform infrared (FTIR) spectra, respectively. A CHI 660D electrochemical workstation (CH Instruments, Shanghai, China) was employed throughout the electrochemical tests. The conventional triple-electrode configuration was used, which consisted of a bare or modified glassy

carbon electrode (GCE, 3 mm in diameter), a saturated calomel electrode (SCE) and a platinum wire as the working, reference and auxiliary electrodes, respectively. Electrochemical impedance spectroscopy (EIS) measurements were carried out in 10.0 mL of a KCl solution (0.1 M) containing $Fe(CN)_6^{4-}$ and $Fe(CN)_6^{3-}$ (1.0 mM) (1:1), with the impedance spectra recorded in a frequency window of 10^5 Hz - 0.1 Hz at the open circuit potential (voltage amplitude: 5 mV). All electrochemical tests were performed under a high-purity nitrogen atmosphere at ambient temperature.

3. RESULTS AND DISCUSSION

As indicated in the FTIR spectra shown in Fig. 1A, oxygen-containing species were produced on the GO during the synthetic process, and a majority of these species remained after the formation of AgNPs on the GO surface. This result suggested that glucose was a mild reductant. Several characteristic absorption bands in both spectra are similar but have nonsignificant variation in their intensities. The peaks at 1384 cm^{-1} and 3446 cm^{-1} correspond to the –OH vibration. There are also bands corresponding to C–O groups (1055 cm^{-1}). The spectra of AgNPs/GO and GO both show weak absorption bands at 1631 cm^{-1}, suggesting the skeletal vibration of the graphene sheets (unoxidized sp^2 C-C bonds). Raman spectroscopy is a common and non-destructive method for the structural characterization of carbon-based materials. AgNPs can interact with GO sheets through physisorption, electrostatic binding or charge transfer interactions [36]. As shown in the Raman spectra in Fig. 1B, the D line at 1350 cm^{-1} and the G line at 1600 cm^{-1} are characteristic properties of GO. The significant D peak at 1350 cm^{-1} with an intensity comparable to that of the G peak at 1600 cm^{-1}, together with the large band width of the two peaks, suggest remarkable disorder in the GO. The *D* band provides information on the breathing mode of the κ-point, and the *G* band relates to the tangential stretching mode of the E_{2g} phonon of an sp^2 carbon atom [37].
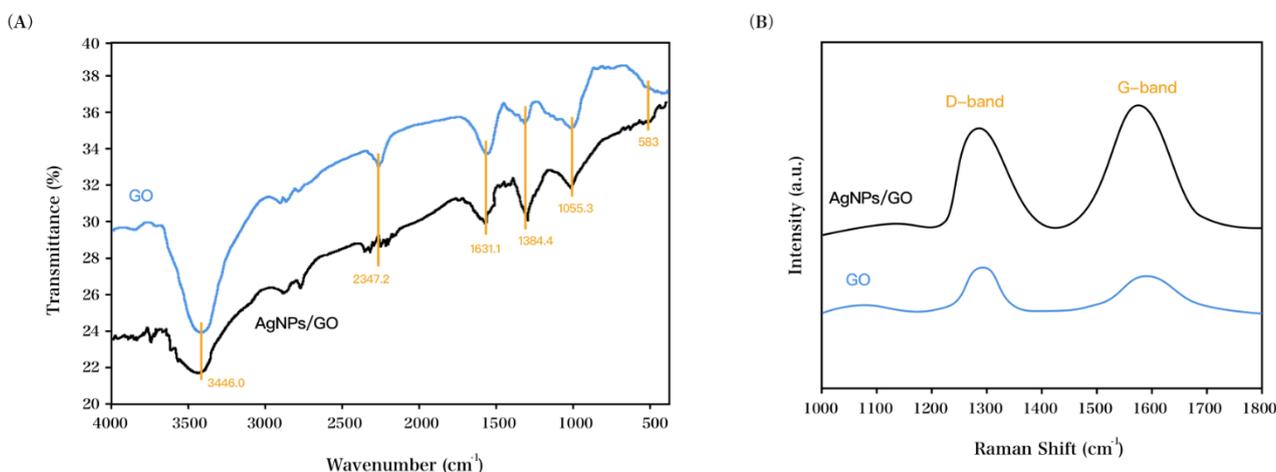

Figure 1. (A) FTIR and (B) Raman spectra of GO and AgNPs/GO.

There is an obvious increase in the Raman intensities of both the D and G bands after the deposition of AgNPs on the GO due to the surface-enhanced Raman scattering (SERS) activity of the AgNPs. The SERS is possibly ascribed to a chemical effect since the attached functional species can

be used as nucleation centers by the AgNPs deposited on the GO sheets. The G line corresponds to the breathing mode of the *k*-point phonons of A_{1g} symmetry, while the G line is ordinarily ascribed to the first-order scattering of the E_{2g} phonons of sp^2 C atoms. There is an obvious increase in the Raman intensities of both the D and G bands of AgNPs/GO, which is ascribed to the SERS activity of the AgNPs. This result is indicative of the successful deposition of AgNPs on the GO.

EIS is a common and effective technique for monitoring the interfacial features of surface-modified electrodes. Ordinarily, the characteristic impedance spectrum is comprised of a semicircle section at higher frequencies and a linear section at lower frequencies. As indicated in Fig. 2, AgNPs/GO/GCE was electrochemically characterized via EIS. The bare GCE exhibited a high R_{ct} of ca. 600 Ω, suggesting a comparatively difficult electron exchange at the bare GCE. The semicircle diameter increased dramatically (R_{ct} = 1000 Ω) after the electrode was modified by GO since interfacial charge transfer was made more difficult by the presence of GO. The total electrode impedance corresponds to the electron transfer resistance (*R*) in series with the parallel connection of the double layer capacitance (*C*) and Warburg impedance (*Z*). In general, a semicircle portion results from the parallel combination of *R* and *C*. The RGO/Ag nanocomposite had a lower *R* value than that of the bare and RGO-modified electrodes, revealing its faster electron transfer ability. The superior conductivities of RGO and Ag lead to faster electron transfer at the nanocomposite-modified electrode surface [38]. This unfavorable phenomenon occurred since the electrostatic repulsion between the negative surface charges of $Fe(CN)_6^{4-/3-}$ and GO hinders the ability of the probe ion to approach the electrode surface for electron exchange, which leads to the resistance increase. This result is consistent with those of recent reports. There was a sharp decrease in the electron transfer resistance when AgNPs/GO was coated on the GCE, with an R_{ct} value of 420 Ω.
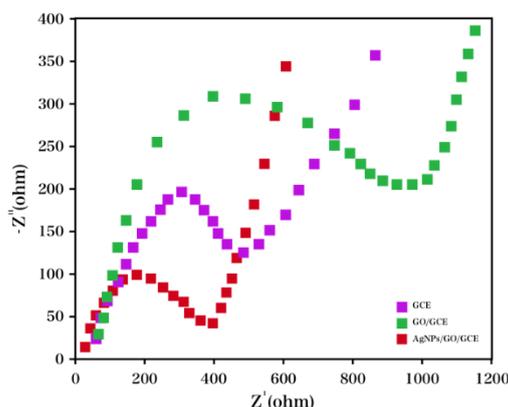

Figure 2. EIS of various electrodes in a 0.1 M KCl solution containing 1.0 mM $Fe(CN)_6^{4-/3-}$ (1:1). The frequency range was 10^5 Hz - 0.1 Hz at the open circuit potential. Voltage amplitude: 5 mV. Inset: equivalent circuit.

TSGF is a relatively new tumor marker associated with vascular proliferation of malignant tumor, which can be the filter predictor for variant cancer [39-41]. CV was used to study the electrocatalytic activity of the AgNPs/GO/GCE towards TSGF oxidation. As shown in Fig. 3, the bare

GCE, the GO/GCE and the AgNPs/GO/GCE before and after the addition of TSGF (0.1 mM) in acetate buffer (0.1 M, pH 4.5) were characterized via CV (scan rate: 50 mV/s). Before the addition of TSGF, the bare GCE and GO/GCE exhibited no redox peaks, suggesting the electrochemically inert nature of the GO film in the selected potential domain. Compared with the bare GCE, the GO/GCE exhibited a higher background current since the GO possessed a large specific area. Before the addition of TSGF, the AgNPs/GO/GCE showed a pair of obvious redox peaks. It was clear that these peaks belonged to the redox reaction of $Ag^{+/0}$ in the nanocomposite, where the oxidization of the electroactive AgNPs to Ag^+ occurred at 0.38 V vs. SCE on the forward anodic scan and Ag^+ was transformed back into Ag at 0.28 V (vs. SCE) on the reverse cathodic scan. This result provided additional evidence for the successful immobilization of AgNPs on the surface of GO. After the addition of TSGF (0.1 mM), the GCE displayed a weak oxidation peak at a comparatively high potential of 1.05 V (vs. SCE) with a lower peak current than that of the GO/GCE. With the immobilization of GO on the GCE surface, there was an increase in the oxidation peak current and a negative shift in the oxidization peak potential, which suggested that TSGF oxidation could be catalyzed by GO. Nevertheless, in comparison with the bare GCE, the AgNPs/GO/GCE displayed a more negative shift in the oxidation peak potential of TSGF. Compared with the GO/GCE, the AgNPs/GO/GCE displayed an obvious increase in the oxidation peak current. These differences suggest that the AgNPs/GO possessed a synergistic effect and could effectively catalyze the electrochemical oxidation of TSGF.
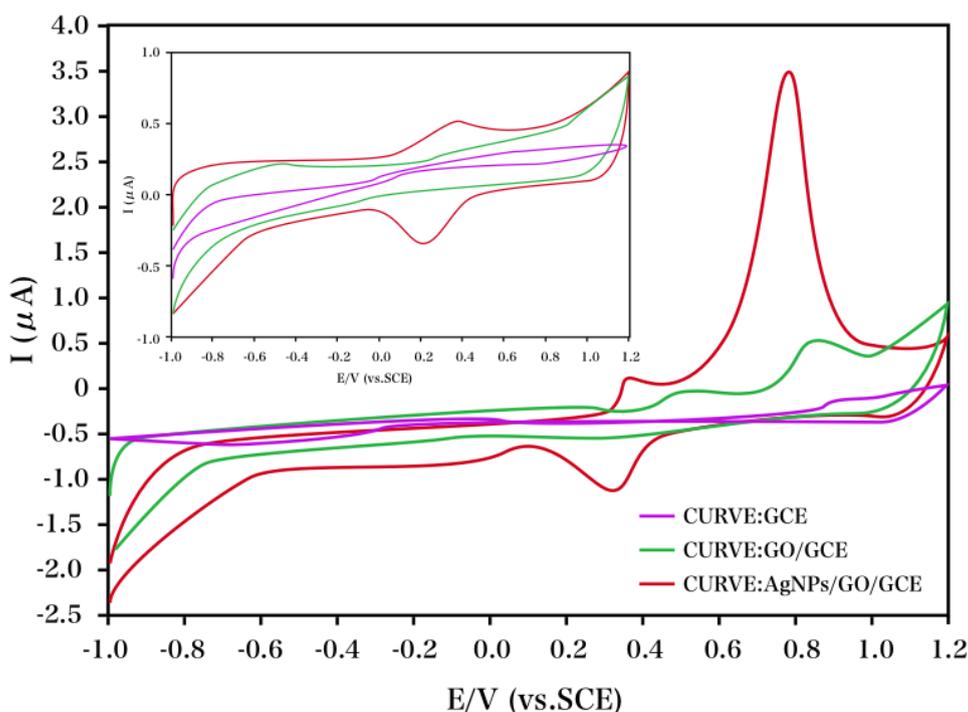

Figure 3. CVs of the various electrodes before and after the addition of TSGF (0.1 mM) in acetate buffer (0.1 M, pH 4.5). Scan rate: 50 mV/s.

CV curves obtained at various potential scan rates provide useful data, including kinetic features and electrochemical mechanisms. TSGF (0.1 mM) was characterized at the AgNPs/GO/GCE nanocomposite via CV at scan rates in the range of 10 - 300 mV/s (Fig. 4A). There was a linear variation of the anodic peak current (i_{pa}) in the selected scan rate range with a slope of and a correlation coefficient of 0.9917 (Fig. 4B). This indicates that an adsorption process controlled the kinetics of the electrode reaction. Interestingly, as the scan rate increased, the oxidation peak potential for TSGF displayed a positive shift. The reduction peak at the electrode increased in current and shifted to a positive potential as the size and density of the AgNPs increased [42]. Fig. 4B displays the relationship between the potential and the natural logarithm of the scan rate (ln v). A linear variation in the potential (vs. ln) was observed over a range of 10 - 300 mV/s. The electrochemical reaction of TSGF at this decorated electrode was a two-electron, two-proton process.
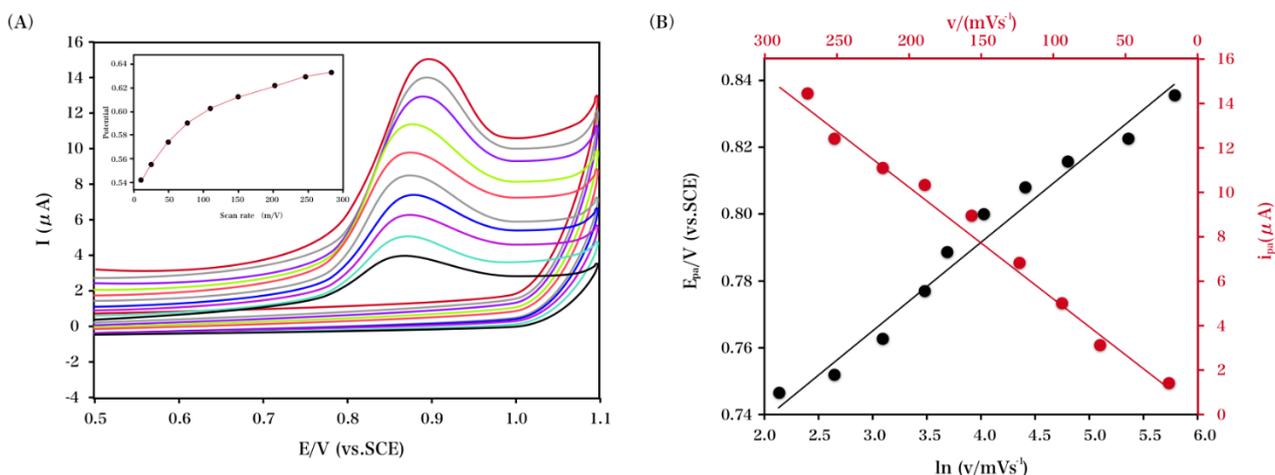

Figure 4. (A) CVs of TSGF (0.1 mM) at the AgNPs/GO/GCE with varied scan rates in acetate buffer (pH 4.5). Inset: plot of E_{pa} vs. v; (B) plots of i_{pa} vs. v and E_{pa} vs. ln v.
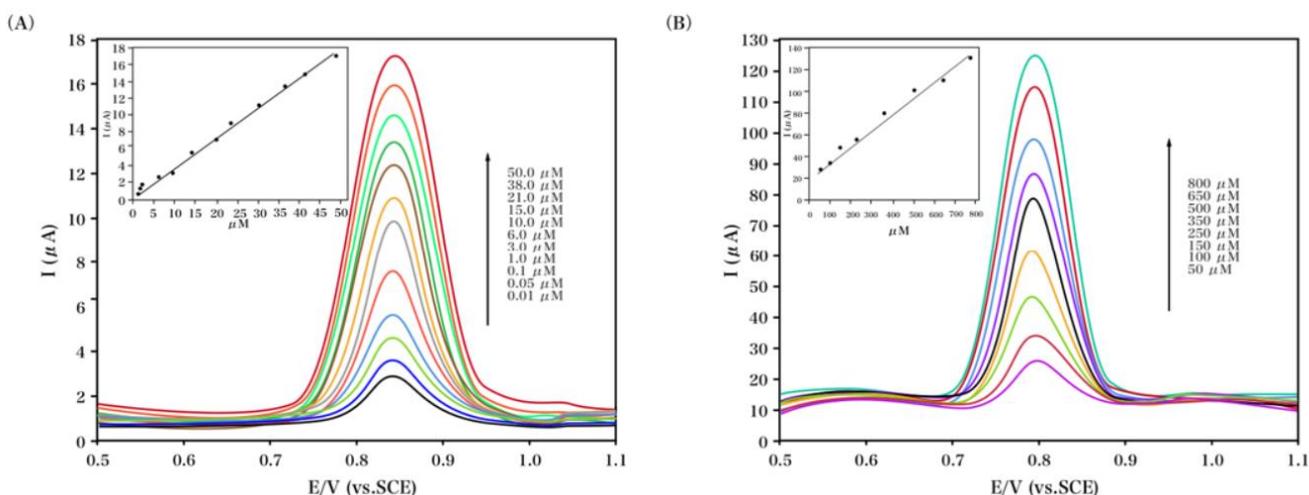

Figure 5. (A) DPVs for the AgNPs/GO/GCE in acetate buffer (0.1 M, pH 4.5) containing low concentrations of TSGF. (B) DPVs for the AgNPs/GO/GCE in acetate buffer (0.1 M, pH 4.5) containing high concentrations of TSGF.

DPV is a common analytical method used to enhance specificity and sensitivity in quantitative measurements. Therefore, DPV was used for TSGF detection with a scanning potential of 0.5 - 1.1 V (differential pulse step potential: 5 mV; modulation amplitude: 5 mV). After the decrease in the background current to a steady value, acetate buffer (0.1 M, pH 4.5) was mixed with TSGF solutions. After a previous accumulation time of 120 s at the open circuit potential, the currents generated due to the electrocatalytic oxidation of TSGF were recorded. There was a linear increase in the oxidation peak currents with increasing TSGF concentration in the ranges of 0.01 µM - 50.0 µM, and 50.0 µM - 800.0 µM (Fig. 5), with a limit of detection (LOD) of 7 nM (S/N=3). To allow for comparison to previous reports, the characteristics of different determination methods for TSGF are summarized in Table 1. Moreover, in the clinical detection in fluids and pharmaceuticals, significant amounts of biological substances, including glucose, uric acid and ascorbic acid, usually coexist with TSGF. The effect of the aforementioned interference agents and other available amino acids was investigated via DPV in acetate buffer (0.1 M, pH 4.5) containing TSGF (1.0 µM). It could be seen from the results that the TSGF signals were not affected by 50-fold higher concentrations of glucose, uric acid and ascorbic acid, and the deviations were 2.7%, 1.7% and 2.4%, respectively. Therefore, the as-prepared sensor possesses anti-interference characteristics and is highly effective in the detection of TSGF at trace levels when possibly interfering groups exist in the complex matrix.

Table 1. Comparison of the major characteristics of determination methods used for the detection of AFP.

Electrode	Linear detection range	Detection limit	Reference
Poly(guanine)-functionalized silica nanoparticle label	0.5 µM - 20.0 µM	0.28 µM	[43]
MB labeled TNF-α aptamer	0.05 µM - 20.0 µM	0.01 µM	[44]
Colorimetric biochemistry kit	0.4 µM - 70.0 µM	0.16 µM	[45]
AgNPs/GO/GCE	0.01 µM - 50.0 µM 50.0 µM - 800.0 µM	7 nM	This work

To investigate the practical application of the as-prepared sensor, human serum and pharmaceutical injections were employed as real specimen models. Through simple needle aspiration, 4 mL of the peripheral blood specimens were obtained. After centrifugation at 2000 rpm for 10 minutes in a desktop centrifuge to remove the cells, the preparation of the specimens was successfully achieved. To avoid any possible matrix effects, the standard addition method was performed for TSGF detection in the real specimens. The recoveries varied within the ranges of 99.0% - 102.7% for the serum and 98.18% - 102.52% for the injection (Table 2). We also used a colorimetric biochemistry kit from Fujian New Continent Biochemical Technology Limited Company as a reference method for comparison. The recovery data was found to be within the desirable range; hence, the proposed sensor is favorably accurate in the detection of TSGF in complex specimens.

Table 2. Characterizations of TSGF detection in human serum specimens via AuNPs/GO/GCE.

Samples	Added (µM)	Found (µM)	Colorimetric kit (µM)	Recovery (%)	RSD (%)
1	0.00	3.22	3.17	–	1.8
	5.00	8.29	8.32	100.86	2.4
	10.00	12.98	12.77	98.18	2.7
2	0.00	2.47	2.51	–	1.6
	10.00	12.50	12.47	100.24	1.9
	20.00	22.05	20.98	99.14	2.4
3	0.00	4.70	4.65	–	1.8
	30.00	35.09	34.71	101.12	3.6
	50.00	56.08	57.22	102.52	4.0

4. CONCLUSION

This work proposed a low-cost method for preparing AgNPs/GO, and a new electrochemical sensor was successfully fabricated using this nanocomposite. The results of electrochemical investigations showed that the AgNPs/GO composite exhibited synergetic catalytic effects on TSGF oxidation, and the dramatic peak current increase and peak potential reduction significantly promoted the analytical behavior of the proposed sensor. Wide linear ranges and a low LOD were obtained under optimal conditions.

References

1. A. Opstal-van Winden, W. Rodenburg, J. Pennings, C. van Oostrom, J. Beijnen, P. Peeters, C. van Gils and A. de Vries, *International Journal of Molecular Sciences*, 13 (2012) 13587.
2. M.S. Ghadge, P.P. Naik, B.P. Tiwari, R.M. Hegde and T.J. Matale, *Indian Journal of Clinical Biochemistry*, 27 (2012) 97.
3. S. Pitteri, L. Amon, T.B. Buson, Y. Zhang, M.M. Johnson, A. Chin, J. Kennedy, C. Wong, Q. Zhang and H. Wang, *Cancer research*, 70 (2010) 8598.
4. Z. Sahab, Y. Man, S. Byers and Q. Sang, *International journal of molecular sciences*, 12 (2011) 4504.
5. S. Zhang, Y. Hu, H. Qian, S. Jiao, Z. Liu, H. Tao and L. Han, *Asian Pacific Journal of Cancer Prevention*, 14 (2013) 3937.
6. N. Boyd, H. Guo, L. Martin, L. Sun, J. Stone, E. Fishell, R.A. Jong, G. Hislop, A. Chiarelli and S. Minkin, *N. Engl. J. Med.*, 356 (2007) 227.
7. F. Mannello, V. Medda and G. Tonti, *Expert Review of Proteomics*, 6 (2009) 43.
8. A. Huijbers, B. Velstra, T. Dekker, W. Mesker, Y. van der Burgt, B. Mertens, A. Deelder and R. Tollenaar, *International Journal of Molecular Sciences*, 11 (2010) 4175.
9. M. Sun, A. Meng, X. Huang and M. Wang, *Asian Pacific Journal of Cancer Prevention*, 14 (2013) 149.
10. E. Piura and B. Piura, *Journal of Oncology*, 2010 (2010)
11. S. Zervoudis, G. Iatrakis, P. Economides, D. Polyzos and I. Navrozoglou, *Women's Health*, 6 (2010) 135.

12. V. Kulasingam, Y. Zheng, A. Soosaipillai, A. Leon, M. Gion and E. Diamandis, *International Journal of Cancer*, 125 (2009) 9.

13. H.L. Hwa, W. Kuo, L. Chang, M. Wang, T. Tung, K. Chang and F. Hsieh, *Journal of Evaluation in Clinical Practice*, 14 (2008) 275.

14. C. Sturgeon, M. Duffy, U. Stenman, H. Lilja, N. Brünner, D.W. Chan, R. Babaian, R. Bast, B. Dowell and F. Esteva, *Clinical Chemistry*, 54 (2008) e11.

15. C. Perou, T. Sørlie, M. Eisen, M. van de Rijn, S. Jeffrey, C. Rees, J. Pollack, D. Ross, H. Johnsen and L. Akslen, *Nature*, 406 (2000) 747.

16. S.. Jiang, H. Chen, S. Dowdy, A. Fu, J. Attewell, E. Kalogera, R. Drapkin, K. Podratz, R. Broaddus and J. Li, *International journal of molecular sciences*, 14 (2013) 22655.

17. M. Xiang, W. Zhou, D. Gao, X. Fang and Q. Liu, *International Journal of Molecular Sciences*, 13 (2012) 16737.

18. C.S. Zhu, P.F. Pinsky, D.W. Cramer, D.F. Ransohoff, P. Hartge, R.M. Pfeiffer, N. Urban, G. Mor, R.C. Bast and L.E. Moore, *Cancer Prevention Research*, 4 (2011) 375.

19. R. Moore, D. McMeekin, A. Brown, P. DiSilvestro, M. Miller, W. Allard, W. Gajewski, R. Kurman, R. Bast and S. Skates, *Gynecologic Oncology*, 112 (2009) 40.

20. S.G. Baker and D.J. Sargent, *Journal of the National Cancer Institute*, (2010)

21. S. Chen, J. Wang, W. Gou, Y. Xiu, H. Zheng, Z.-H. Zong, Y. Takano and Y. Zhao, *International Journal of Molecular Sciences*, 14 (2013) 24187.

22. B. Yu, P. Xu, Q. Wang, H. Zhou and H. Zhou, *Journal of International Medical Research*, 37 (2009) 878.

23. J. Jiang, C. Wu, H. Deng, M. Lu, J. Wu, H. Zhang, W. Sun and M. Ji, *World Journal of Gastroenterology*, 10 (2004) 1675.

24. B. Li, T. Liu, Y. Wang and Z. Wang, *Journal of Colloid and Interface Science*, 377 (2012) 114.

25. J. Li, D. Kuang, Y. Feng, F. Zhang, Z. Xu and M. Liu, *J. Hazard. Mater.*, 201 (2012) 250.

26. S. Yu, G. Zou and Q. Wei, *Talanta*, 156 (2016) 11.

27. X. Yan, K. Wang, W. Lu, W. Qin, D. Cui and J. He, *Nanoscale Research Letters*, 11 (2016) 138.

28. H. Yin, A. Blichfeld, M. Christensen and B. Iversen, *ACS Applied Materials & Interfaces*, 6 (2014) 10542.

29. X. Xing, S. Liu, J. Yu, W. Lian and J. Huang, *Biosensors and Bioelectronics*, 31 (2012) 277.

30. S. Stankovich, D. Dikin, R. Piner, K. Kohlhaas, A. Kleinhammes, Y. Jia, Y. Wu, S. Nguyen and R. Ruoff, *Carbon*, 45 (2007) 1558.

31. D.A. Dikin, S. Stankovich, E. Zimney, R. Piner, G. Dommett, G. Evmenenko, S. Nguyen and R. Ruoff, *Nature*, 448 (2007) 457.

32. J. Robinson, F. Perkins, E. Snow, Z. Wei and P. Sheehan, *Nano Letters*, 8 (2008) 3137.

33. Y. Guo, B. Wu, H. Liu, Y. Ma, Y. Yang, J. Zheng, G. Yu and Y. Liu, *Adv. Mater.*, 23 (2011) 4626.

34. Q. Bao, D. Zhang and P. Qi, *Journal of Colloid and Interface Science*, 360 (2011) 463.

35. M. Hirata, T. Gotou, S. Horiuchi, M. Fujiwara and M. Ohba, *Carbon*, 42 (2004) 2929.

36. B. Yang, Z. Liu, Z. Guo, W. Zhang, M. Wan, X. Qin and H. Zhong, *Applied Surface Science*, 316 (2014) 22.

37. F. Schedin, E. Lidorikis, A. Lombardo, V. Kravets, A. Geim, A. Grigorenko, K. Novoselov and A. Ferrari, *ACS Nano*, 4 (2010) 5617.

38. S. Palanisamy, C. Karuppiah and S. Chen, *Colloids and Surfaces B: Biointerfaces*, 114 (2014) 164.

39. M. Shamsipur, L. Farzin, M. Tabrizi and F. Molaabasi, *Biosensors and Bioelectronics*, 74 (2015) 369.

40. M. Mazloum-Ardakani, L. Hosseinzadeh and Z. Taleat, *Microchimica Acta*, 181 (2014) 917.

41. Y. Wu, X. Na, Y. Zang, Y. Cui, W. Xin, R. Pang, L. Zhou, X. Wei, Y. Li and X. Liu, *Biochemical and Biophysical Research Communications*, 449 (2014) 502.

42. F. Lorestani, Z. Shahnavaz, P. Mn, Y. Alias and N.. Manan, *Sensors and Actuators B: Chemical*, 208 (2015) 389.

43. J. Wang, G. Liu, M.H. Engelhard and Y. Lin, *Analytical Chemistry*, 78 (2006) 6974.
44. Y. Liu, Q. Zhou and A. Revzin, *Analyst*, 138 (2013) 4321.
45. B. Deng, Q. Tan, X. Fan, Y. Jiang, Y. Zhao, J. Zhou, Y. Liang and R. Wang, *Clinical Lung Cancer*, 12 (2011) 192.